Applied Physics A (2023) 129:462
https://doi.org/10.1007/s00339-023-06736-5

Applied Physics A
Materials Science & Processing

Cancer targeted contrast studies and photothermal therapy using engineered gold nanoparticles

S. Vijayakumar[1]

Received: 26 February 2023 / Accepted: 20 May 2023 / Published online: 2 June 2023
© The Author(s), under exclusive licence to Springer-Verlag GmbH, DE part of Springer Nature 2023

Abstract

In biomedical applications, gold nanoparticles (AuNps) plays an excellent role in drug delivery and carrier for anticancer agent. They exhibit increased permeability and retention in tumours, Surface Plasmon Resonance in near-infrared light, and ability to be conjugated with pharmaceuticals. They also produce secondary electrons when interacting with radiation. Existing cancer diagnosis and treatment mechanisms, however, do not always extend the lives of cancer patients. There are several negative consequences of current approaches, such as adverse effects and an increased risk of relapse. In more environmentally friendly manner, *soursop* fruit extracts are used to create and stabilise gold nanoparticles. Several methods, including UV–Visible spectroscopy, Transmission Electron Microscopy, Fourier Transform Infrared Spectroscopy, and Zeta potentiometer were used to characterise the nanoparticles. These particles are readily soluble in water, long-lasting, and effective against the MCF-7 breast cancer cell line. Pharmacokinetics, photothermal treatment, and molecular cancer imaging using gold nanoparticles have all been effectively proven. Compared to its untargeted cousin, the molecularly targeted tumour exhibits greater contrast. Gold nanoparticle accumulation has been reported to be highest in breast tumours. Gold nanoparticles exposed to laser radiation at the tumour location and permanently damaged tumour tissue without killing healthy cells. A 5-month follow-up revealed no evidence of tumour recurrence in the rats treated with gold nanoparticles and laser.

Keywords Gold nanoparticles · *Soursop* · Breast cancer · Contrast · Pharmacokinetics · Photothermal therapy

1 Introduction

Over millennia, the biological matter has been mainly composed of nanoscale components such as working cells, biological entities, bacteria, and viruses. Nanotechnology has played an influential role in the field of medical science for the last decade and is a promising field for new applications [1]. More surface area of nanoscale materials leads to rapid sensing of chemical entities as compared to their bulk counterparts. In a healthy body, the natural system controls the creation, growth and death of cells. However, when these systems malfunction more cell growth than death can occur, resulting in a malignant tumour or cancer. Developments in nanomedicine have the potential to create implants that can monitor the chemistry of the system and release drugs whenever required. Gold nanoparticles (AuNps) can be used for cancer treatment, biological imaging, chemical sensing, and drug delivery [2]. Interestingly, AuNps can act as a contrast agent and dose enhancer in image-guided nanoparticle-enhanced radiotherapy using kilovoltage cone-beam computed tomography [3, 4].

Tri-iodobenzene with pharmaceutical additives is a basic X-ray contrast agent. The contrast agent diatrizoate was first introduced in 1954, but it is a source of chemotoxicity due to its high osmolality 1.57 OSM Kg^{-1} for 300 mg of solution. AuNps and iodine agents enclosed in liposomes are another X-ray contrast agents [5]. Comparing AuNps to iodine contrast agents, the contrast level of AuNps are almost three times higher [6]. The early detection, diagnosis, and treatment of the disease are crucial for its recurrence frequency after therapy, and mortality rate [7–9]. Thus, it is crucial and required to develop methods for spotting cancer in its earliest stages. On-time therapeutic medication and genetic material delivery to sick tissues has been achieved using AuNps [10–12]. Some of the top leading types of cancer with increased cancer-associated death are lung, colorectal, stomach, liver, breast, oesophageal, pancreas, and prostate

✉ S. Vijayakumar
vijaysk.research@gmail.com

[1] Department of Science and Humanities, Karpagam College of Engineering, Coimbatore, India

[13]. In recent years, much success has been achieved in cancer treatment. The primary treatment modalities for cancer treatments are surgery, chemotherapy, and radiotherapy [14]. The choice of treatment depends on the tumour type, location, histological type, size, stage and the level of metastasis [15, 16] Cancer cells have the potential not to undergo apoptosis and are characterized by aggressive cell proliferation compared to non-cancerous cells [17]. Cancer metastasis and treatment resistance work hand in hand to invade their surrounding tissues. Once they have evaded they continue to metastasize and migrate to other tissues [18].

In 1700 BC, a glowing point from a fire drill was used for breast cancer treatment [19]. Later heating sources such as radiofrequency [20], microwaves [21] and ultrasound waves [22] were introduced to induce moderate heating in a specific target region, which is termed hyperthermia. Hyperthermia is a photothermal therapy with the support of nanoparticles for a temperature range 41 °C–50 °C using radiofrequency, ultrasound and microwaves [23]. Tumours cannot withstand such high temperatures because of the rapid rise in temperature of the metallic nanoparticles present in the tumour. Denaturing proteins and loosening cell membranes are irreversible effects of hyperthermia. Due to the reduced tolerance of cancer cells compared to normal tissues and due to the poor supply of blood in the tumour, hyperthermia can smash the tumour in a site-specific manner without ruining healthy cells. The extensive potential applications and biocompatibility, AuNps have been used in early clinical trials [24]. AuNps offer a significant route to targeting only cancerous cells without affecting the healthy cells [25]. The multidisciplinary approach and applications of gold nanoparticles are referred in Fig. 1.

2 Materials and methods

Materials used for the synthesis of AuNps are hydrogen tetrachloro aurate ($HAuCl_4.H_2O$) purchased from Sigma Aldrich, Coimbatore, India. Extracts of *Soursop* are prepared using double-distilled water. In vitro, assay reagents such as Phosphate buffer saline (PBS), Trypsin-Ethylenediaminetetraacetate Acid (EDTA), Foetal bovine serum (FBS), and Dimethyl sulphoxide (DMSO) are purchased from Sigma Aldrich, India. Chemicals and solvents are reagent grade and are used. without further purification. In the current study, Sprague Dawley rats (Female) are used for the experimental purposes. The permission for animal experiments obtained from the Committee for Control and Supervision of experiments on Animals (CPCSEA) and the Institutional Animal Ethics Committee (IAEC). [Proposal Number. KMCRET/TSCST/01/2014– 2015. Registration Number. 685/Po/02/a/CPCSEA/, Dated 21 August 2002, IAEC No. KMCRET/TSCST/01/3014-2015].

Animals are grouped into six groups and each group has eight rats. The first two groups are the control group; the third and fourth groups are injected with AuNps for contrast studies. The fifth and sixth groups are injected with AuNps for photothermal therapy. Laser therapy uses near-IR light at wavelengths of 700–800 nm. AuNps are administered through the tail vein of Female Sprague Dawley rats. This enables these nanoparticles to eradicate targeted tumours. When laser light is applied to a tumour containing gold nanoparticles, the particles heat up rapidly and kill the tumour cells.

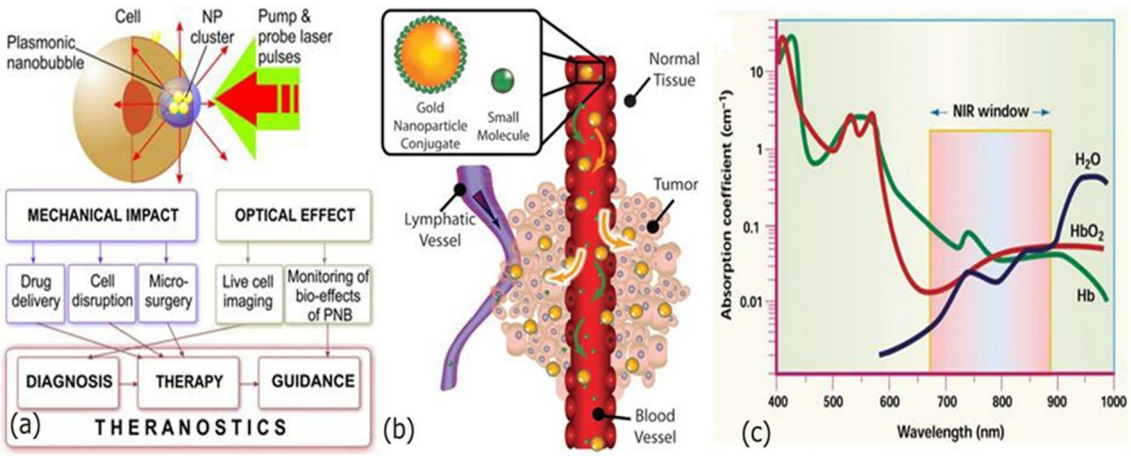

Fig. 1 Schematic representation of (**a**) biomedical applications of gold nanoparticles in different fields, (**b**) Graphic illustrating the size-selective preferential accumulation of circulating gold nanoparticle conjugates at tumour sites by the enhanced permeability and retention (EPR) effect. (**c**) Wavelength range of the near-infrared (NIR) tissue transmission window [26]

3 Characterization of gold nanoparticles

Characterization is necessary to establish an understanding and control of nanoparticle synthesis and applications. AuNps synthesized using *soursop* fruit extract was characterized by Ultraspec-3000 series UV–Visible spectrophotometer (Nanoscience and Nanotechnology Department, Sri Ramakrishna Engineering College, Coimbatore, India) to study the peak absorption band. The formation of AuNps at a particular wavelength was confirmed by UV–Visible spectroscopy, which utilizes a localized Surface Plasmon Resonance (SPR) band. When a metal particle is exposed to light, the oscillating electromagnetic field causes a collective coherent oscillation of the metal's free electrons. This electron oscillation across the particle surface generates charge separation concerning the ionic lattice. This results in a dipole oscillation parallel to the light's electric field direction. The oscillation amplitude is greatest at a specific wavelength, known as Surface Plasmon Resonance (SPR) [27].

High-Resolution Transmission Electron Microscopy, JEOL JEM 2100 operating at an accelerating voltage 200 kV with a lattice resolution 0.14 nm and point-to-point resolution of 0.19 nm (PSG Institute of Advanced Studies, Coimbatore, India) was used to confirm the formation of AuNps, identify particle distribution and size range. The crystalline nature of nanoparticles was identified with the help of the Selected Area Electron Diffraction (SAED) pattern. The AuNps images were formed from the interaction of electrons transmitted through the thin film of a specimen. Zeta potential measures the effective electric charge on a nanoparticle surface and quantifies it. Zeta potential was found to be a determinant of particle stability. Zeta potentials increase in magnitude as electrostatic repulsion increases, thus increasing stability. Zeta potential measurement was performed using Malvern Instruments Zeta sizer 1000 Hs operating with variable power (5–50 mW) He–Ne laser at 633 nm (Sri Ramakrishna Engineering College, Coimbatore). Fourier Transform Infrared Spectroscopy (FTIR) spectrum was recorded using the SHIMADZU FTIR spectrometer, and the FTIR spectra of the sample were recorded in the KBr phase in the frequency region of 10,000—400 cm^{-1}. The MTT cytotoxicity assay of AuNps capped with *soursop* on breast cancer cell lines was analyzed at KMCH Pharmacy College, Coimbatore.

4 Experimental

4.1 Preparation of gold nanoparticles and intravenous injection in rat

The preparation of AuNps functionalized with phytochemicals is as per the protocol followed in our previous publication [28]. AuNps is a novel agent, which enables enhanced X-ray imaging of blood vessels, kidneys, tumour and other organs. 10 ml AuNps solution is mixed with a buffer solution. The nanoparticles are filtered through 0.2-micron filter paper and centrifuged for 8 min. To ensure maximum recovery, a second and third filtration was performed by adding 15 µl of buffer solution. About 0.2 ml of AuNps solution was injected through the tail vein of female Sprague Dawley rats. It was found that the skin, ears, eyes and paws became darker due to the gold nanoparticles present in the blood vessels of a rat.

4.2 Cytotoxicity study

The human breast cancer cell lines (MCF) were grown in an Eagle medium containing 10% foetal bovine serum (FBS). The cells were incubated at 37 °C with 5% CO_2 to have 100% relative humidity in 95% air. To make a single-cell suspension, the monolayer cells were detached with trypsin-ethylene diamine tetra-acetic acid (EDTA). The viable cells were counted using a spectrophotometer and diluted with a medium containing 5% FBS to give the final density 1×10^5 cells/mL. The cytotoxicity evaluation of AuNps was performed using MTT assay as described by Mossman [29]. About 1×10^5 mL^{-1} cells of MCF-7 in their experimental growth phase were seeded in a flat-bottomed 96-well polystyrene-coated plate and incubated for cell attachment. After 24 h, the cells were treated with a serial concentration of (0, 20, 40, 60, 80, 100, and 120) mg/mL of the test samples. For making the final concentration, aliquots of 100 µl of these different sample dilutions were added to the appropriate wells already containing 100 µl of a medium. Following the addition, the plates were further incubated for an additional 48 h. The medium without samples served as a control. After 48 h incubation, 15 µl of MTT (5 mg/mL) in phosphate-buffered saline (PBS) was added to each well and incubated at 37 °C for 4 h. The medium with MTT was after flicked off, and the Formosan crystals were solubilized in 100 µL of DMSO and then measured the absorbance at 570 nm using a microplate reader. A percentage of cell viability was calculated with respect to control.

5 Results and discussions

The reduction of hydrogen tetra-chloroaurate into AuNps during exposure to *soursop* fruit extracts could be identified by colour change. Due to the SPR phenomenon, AuNps show a wine-red colour in an aqueous solution. The observed results are highly intriguing for discovering suitable reducing and capping agents for ecologically friendly AuNps synthesis. Chloroauric acid may have been reduced by the flavonoids found in the plant extract, which are potent reducing agents [30]. To adhere to the surface of AuNps and stabilise them by electrostatic repulsion, the carboxylate group can function as a surfactant [31, 32]. Figure 2a illustrates the nanoparticles' Transmission Electron Microscope (TEM) image, which reveals a homogeneous size distribution. Figure 2b shows that the SPR peak absorption was at 526 nm. Elemental analysis is shown in Fig. 2c, the average size of the AuNps was estimated to be 28 nm using a size histogram, Fig. 2d. The diffraction patterns obtained for AuNps are (1 1 1), (2 0 0), (2 2 0) and (3 1 1) which are face-centred-cubic (FCC) structure of nanoparticles. The corresponding *d*-spacing are calculated as 2.40 Å, 2.05 Å, 1.467 Å and 1.22 Å. The SAED in Fig. 2e shows that the samples have crystalline AuNps as deciphered from diffraction pattern using X-rays.

FTIR can be used to determine the nature of molecules associated with plant extracts and nanoparticles. The FTIR spectrum is shown in Fig. 3. As noted above, the functional groups include the primary amino group, ester moiety, mono-substituted benzene ring and carboxylic group [33]. The sharp peaks at 1639.49 cm^{-1} and pulse at 1546 cm^{-1} were assigned to the C=O stretching vibration (amide I) and a mixed vibration of NH deformation and CN stretch (amide II) in amides respectively. In addition, the IR bands at approximately 3371.59 cm^{-1} could also be observed which may be assigned to an O–H stretching vibration in the carboxyl moiety. By contrast, the absorption band corresponding to amide II on the IR spectrum of AuNps was broadened and blue shifted to 1560 cm^{-1}. In contrast, the band corresponding to amide was broadened and red-shifted to 1620 cm^{-1}.

Another feature of AuNps was the presence of a strong and broad band centred at 3440 cm^{-1}. In the literature [34], this band was attributed to various stretching vibrations. An association between the hydrogen bonding of O–H–O

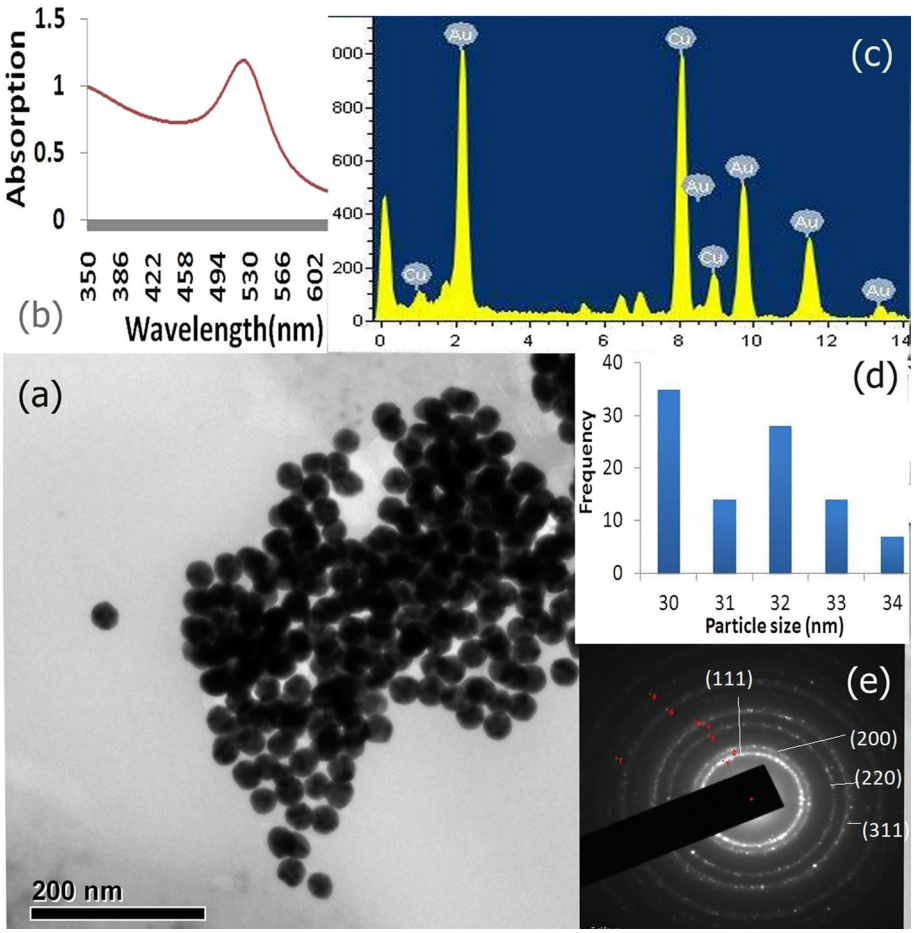

Fig. 2 TEM image of the nanoparticles shows uniform distribution in size, (**b**) SPR peak absorption was found to be 526 nm, (**c**) an elemental analysis of gold nanoparticles, (**d**) an average size of the AuNps was estimated to 28 nm using a size histogram and (**e**) SAED of gold nanoparticles

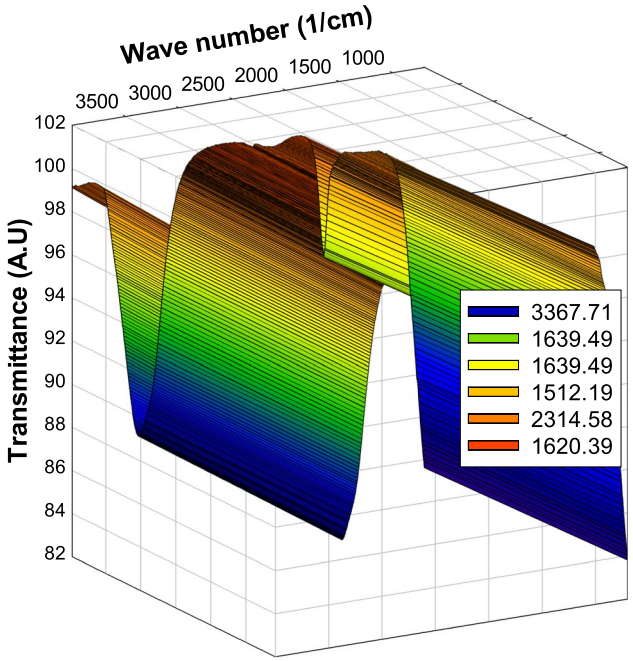

Fig. 3 FTIR spectrum of gold nanoparticles stabilized with *soursop* fruit extract

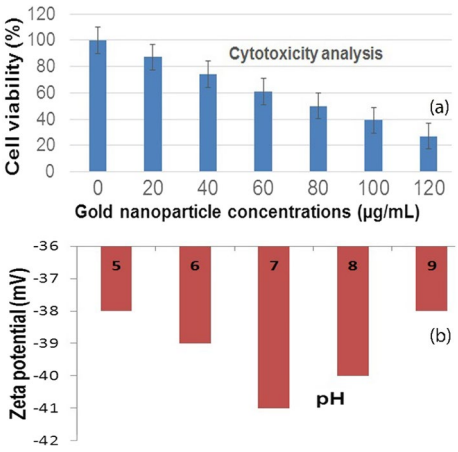

Fig. 4 Cell lines in the exponential growth phase were exposed to different concentrations of AuNps stabilized with *soursop* extract. Cell viability was determined by the MTT assay as described in the experimental section. Each result represents the mean viability ± standard deviation (SD) of three independent experiments and each of these was performed in triplicate. Cell viability was calculated as the percentage of viable cells compared to untreated controls. (**b**) Stability of gold nanoparticles was analyzed with Zeta potentiometer

and the stretching of the ester moiety was identified. Most importantly the peak at 1380 cm^{-1} was assigned to the bending of a methyl group, 1226 cm^{-1} was assigned to C–O stretching of an ester group and 1260 cm^{-1} was assigned to the C–O stretching of a methoxyl group. Further IR clusters from 2800 to 3200 cm^{-1} are attributed to aromatic CH of monosubstituted benzene. Also, intense bands of C–O stretches in the ester moiety were identified at 1735 cm^{-1} and 1732 cm^{-1}. It was thus concluded that chemical constituents of fruit extracts could serve as a reducing and stabilizing agent. The spectra also exhibit an intense band at 1640 cm^{-1} assigned to the N–H stretching band in the free amino groups of biomolecules.

In MTT assay, the sample was capable of metabolizing a dye (3-(4, 5- dimethylthiozol-2-yl)-2, 5-diphenyl tetrazolium bromide) efficiently and the purple-coloured precipitate which is dissolved in a detergent was analyzed spectrophotometrically. After 24 h of post-treatment, MCF-7 cells showed cell viability, which depends on the concentration of AuNps as shown in Fig. 4a. In summary, these results demonstrate that AuNps capped with *soursop* extracts act upon cancer cell lines and destroy them by influencing chemical reactions. The notable toxicity of gold nanoparticles concerning concentration provides new opportunities for the safe application of gold nanoparticles in molecular therapy. *Soursop* capped AuNps treated MCF-7 cells exhibited higher cell death at higher concentrations but in biomedical applications, lower concentration of drug has been used.

The LD_{50} of the fruit extract indicated that it was relatively safe with no mortality recorded. There was no significant ($P > 0.05$) difference in the serum level of alkaline phosphatase (ALP), alanine aminotransferase (ALT) and aspartate aminotransferase (AST) for the liver function test. In a related effect no significant variation recorded on the kidney function parameters [35].

The results of this study suggest that the cytotoxicity of green synthesized gold nanoparticles stabilized with *soursop* was increased with increasing concentration. In addition, it has a strong anticancer effect, according to a literature review. The IC_{50} value of AuNps stabilized with *soursop* is 92 ± 4 µgm/mL. Particle stability is more significant in biomedical applications. The synthesised AuNps were very stable over a range of pH values as shown in Fig. 4b.

X-ray contrast agents have not improved fundamentally over the past three decades. The iodine based contrast agent has not been replaced, despite its serious limitations in medical imaging, including short imaging time, renal toxicity, the need for catheterization and poor contrast in large patients. Gold nanoparticles (AuNps) have been introduced to overcome this limitation. The side effects of iodine agents are caused by high osmolality. Iodine agents contain only three (monomer) or six (dimer) iodine atoms per molecule. By contrast, 28 nm diameter spherical AuNps contain approximately 250 Au atoms. Since AuNps have a low osmolality of 7.2 mM, iso-osmolality can be obtained by further saline addition. Another benefit for intravenous injections is the low viscosity of AuNP solutions. When used with different biofluids, AuNps has significant benefits as a powerful

X-ray contrast agent. Compared to iodine, AuNps has a better absorption coefficient and interacts with bones and tissues less, resulting in a revamped contrast at lower doses. Nanoparticles can stay in the circulation for a longer period of time than low molecular weight iodine solutions, which benefits from longer imaging times [36].

Each of the six groups of animals contains eight rats. For contrast investigations, one rat is used from each group. In the initial investigation, gold nanoparticle pharmacokinetics and contrast levels were tested. At minutes 5, 30, 60, 90, and 120 following injection of the gold nanoparticles, X-ray images of the cancer-prone rats were taken. Female Sprague Dawley rats diseased with cancer cells are injected with AuNps that are 28 nm in diameter through the tail vein. The AuNps are suspended in phosphate-buffered saline (PBS). Direct imaging of the microvascular areas at the tumour site was made possible by the AuNps.

The tumour bearing rats were previously injected with gold nanoparticles before the time slot for X-ray. The tests probed the capability to detect small vessels. The first part of the study concerned with AuNps having an average size of 28 nm. These nanoparticles possess favourable physical characteristics for high-resolution imaging. They are small but monodispersed and have high colloidal stability.

The tumour part of the tissue did not show evidence of particle aggregation, which could otherwise affect the flow and filling of very small microvessels. The X-ray microscopy images are shown in Fig. 5 and demonstrate that these nanoparticles were indeed perfused into a subcutaneous tumour and muscle vessels. These animal studies demonstrate that AuNps are useful as X-ray contrast agents, offering novel physical and pharmacokinetic advantages over typical Iodine-based agents. They provide higher contrast and enable longer imaging times than standard Iodine-based agents. Due to the presence of gold nanoparticles, the broken blood vessels in the tumour are seen in Fig. 5a,c,e,g,i but are not seen in the untreated tumour as shown in Fig. 5b,d,f,h. Reconstructed X-ray images for

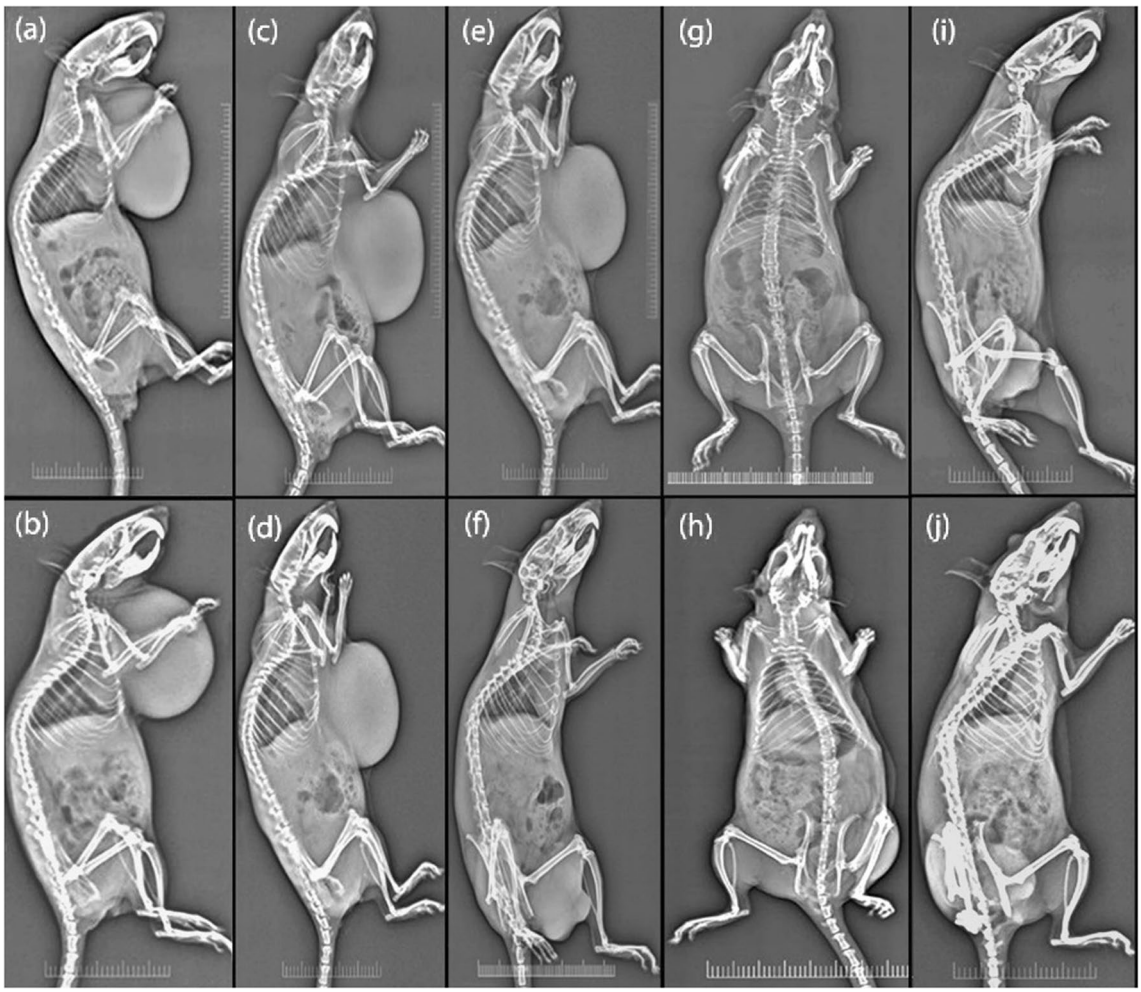

Fig. 5 Pharmacokinetics of gold nanoparticles contrast agent (**a**, **c**, **e**, **g**, **i**) before injection, (**b**) 5 min, (**d**) 30 min (**f**) 60 min (**h**) 90 min and (**j**) 120 min after injection. The AuNps shows biodistribution, pharmacokinetics and high contrast in rat even after two hours of time

untreated and nanoparticle-treated samples are shown in the Fig. 6.

Hyperthermia is known to induce apoptotic cell death in many tissues and has been shown to increase overall survival in amalgamation with chemotherapy and radiotherapy in clinical trials [37]. With heat generation by radiofrequency waves, microwaves, or ultrasound, hyperthermia is usually used in conjunction with other treatments, including radiotherapy. Tumour vasculature constricts, allowing some tumour selectivity, whereas normal tumour vasculature dilates to dissipate heat.

However, overall a lack of specificity for tumour tissue, difficulties in heating deep tumours to therapeutic temperatures and thermotolerance after initial treatment have limited the use of hyperthermia in cancer treatment [38]. Due to their exceptional efficiency at coupling light to SPR frequencies, which leads to strong light absorption, light-to-heat conversion, and heat dissipation thus gold nanoparticles are excellent photothermal agents. The particle type and concentration have an impact on how effectively they can produce heat. Because higher temperatures could be obtained when using gold nanoparticles in photothermal therapy. This study found that there was the greatest effect on cell viability. Smaller nanoparticles may be more effective due to improved photothermal efficiency, improved cellular uptake, or a combination of the two. Gold nanoparticles with the right size, stability, and optical characteristics are looked for potential photothermal therapy. The primary particle criteria were NIR absorbance.

Induced by IR-laser radiation, each selected and scanned rat received a continuous dose of IR-laser radiation for about 1–2 min on the identified tumour spot. On each day, the tumour size was recorded. Each day from the beginning of the treatment, found that the size of the tumour decreased exponentially, Fig. 7a. There was no sign of a tumour after day 26. In addition, the lifespans of the rats were monitored. The rats treated with control and nanoparticles alone died before the 25th day. Even five months after treatment with IR laser plus AuNps, the rats survived. The observed data are plotted in Fig. 7b.

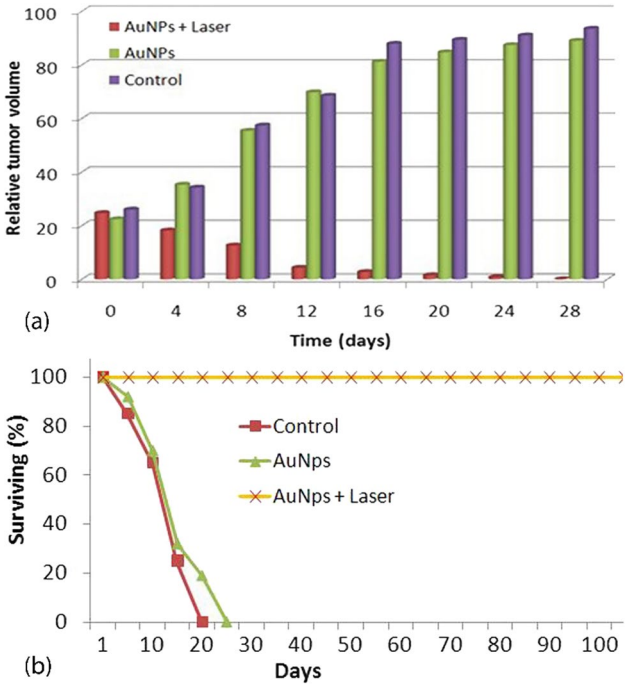

Fig. 7 Tumour size after photothermal treatment for different groups. At day 28, the AuNP+Laser treated tumours underwent complete necrosis while two control groups did not show the same results indicating the feasibility of gold nanoparticles for photothermal therapy

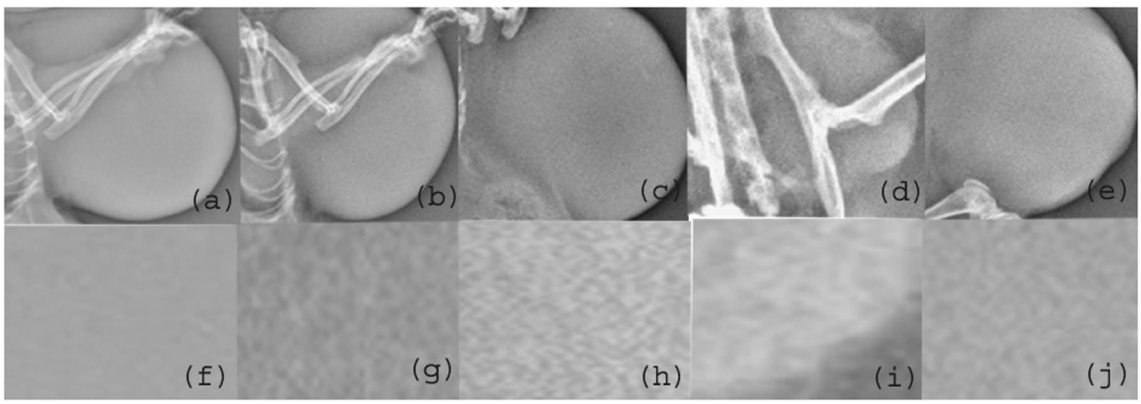

Fig. 6 Reconstructed X-ray micrographs of the microvasculature of tumour in rat. There is microvasculature diffusion of gold nanoparticles in the tumour bearing rat which enhances the contrast level seen in the X-ray image (**b**–**e**) and (**g**–**j**). But this is not clearly seen in untreated rat (**a**, **f**)

6 Conclusion

In conclusion, metal gold nanoparticles were synthesized and stabilized using *soursop* fruit extract in a greener way. The nanoparticles were characterized using various techniques like UV–Visible spectroscopy, Transmission Electron Microscopy, Fourier Transform Infrared Spectroscopy and Zeta potentiometer. These particles are easily soluble in water and stable for more than 5 months. The AuNps are viable in the breast cancer cell line MCF-7. At higher concentrations, there is a visible cytotoxic effect but lower concentration of drugs have been used in biomedical applications. In this study, gold nanoparticle based molecular cancer imaging, pharmacokinetics, and photothermal therapy were demonstrated effectively. A molecularly targeted tumour was more visible than an untargeted tumour. This primary research will pave the way for a future study to characterize critical parameters, such as optimal dosing and detection limits. As nanomedical research advances, metal nanoparticles may be targeted specifically at tumour cells. An in vivo study demonstrated that 28 nm gold nanoparticles maximally accumulated in human breast tumours after intravenous (IV) injection. Laser irradiation of gold nanoparticles at the tumour site caused irreversible damage to the cancerous cells. Over 5 months have passed without any evidence of tumour recurrence in AuNps + Laser treated rats. This targeted treatment clearly demonstrated the destruction of tumours without damaging the healthy cells.

Acknowledgements This work was funded by Tamil Nadu State Council for Science and Technology, Government of Tamil Nadu, India. The author acknowledge the Management and Principal, Karpagam College of Engineering. Sincere thanks to Dr. S. Harihara Sivakumar, KMCH Pharmacy College, Coimbatore for providing facilities, animal housing and support to execute the research work successfully.

Funding This work was supported by the Tamil Nadu State Council for Science and Technology, Government of Tamil Nadu [Grant numbers TNSCST/S&T Projects/AR/PHY/2011-2012/2124, 2012].

Data availability There is no separate data available for this research work.

References

1. K. Zdenka, Phys Med Biol. **63**, 27 (2018)
2. A. Abdulle, J.C.L. Chow, Nanomaterials **9**, 920 (2019)
3. Y. Chen, J. Yang, S. Fu, J. Wu, Int J Nanomed. **15**, 9407–9430 (2020). https://doi.org/10.2147/IJN.S272902
4. A. Tudda, E. Donzelli, G. Nicolini, S. Semperboni, M. Bossi, G. Cavaletti, R. Castriconi, P. Mangili, A.D. Vecchio, A. Sarno, G. Mettivier, P. Russo, Med Phys. **49**(1), 568–578 (2022)
5. L. Liu, L. Cheng, Y. Song, B. Liu, S. Dong, Langmuir **17**, 6747–6750 (2001). https://doi.org/10.1021/la010784
6. K. Dong, Z. Liu, Z. Li, J. Ren, X. Qu, Adv. Mater. **25**, 4452–4458 (2013). https://doi.org/10.1002/adma.201301232
7. J.L. Li, L. Wang, X.Y. Liu, Z.P. Zhang, H.C. Guo, W.M. Liu, S.H. Tang, Cancer Lett. **274**, 319–326 (2009). https://doi.org/10.1016/j.canlet.2008.09.024
8. M. Gobin, M.H. Lee, N.J. Halas, W.D. James, R.A. Drezek, J.L. West, Nano Lett. **7**, 1929–1934 (2007)
9. R. Hong, G. Han, J.M. Fernández, B.J. Kim, N.S. Forbes, V.M. Rotello, J Am Chem Soc. **128**, 1078–1079 (2006)
10. P. Ghosh, G. Han, M. De, C.K. Kim, V.M. Rotello, Adv Drug Deliv Rev. **60**, 1307–1315 (2008)
11. G. Sonavane, K. Tomoda, K. Makino, Colloids Surf B. **66**, 274–280 (2008)
12. J. Ferlay, M. Colombet, I. Soerjomataram, C. Mathers, D.M. Parkin, M. Piñeros, A. Znaor, F. Bray, Int. J. Cancer. **149**, 778–789 (2019)
13. S.M. Smith, K. Wachter, R.L. Schilsky, D.J. George, D.E. Peterson, M.L. Johnson, M.J. Markham, K.F. Mileham, M.S. Beg, J Clin Oncol. **39**, 1165–1184 (2021)
14. J.A. Ajani, T.A. D'Amico, D.J. Bentrem, J. Chao, C. Corvera, P. Das, C.S. Denlinger, P.C. Enzinger, P. Fanta, F. Farjah, J. Natl. Compr. Canc. Netw. **17**, 855–883 (2019)
15. W.J. Gradishar, M.S. Moran, J. Abraham, R. Aft, D. Agnese, K.H. Allison, B. Anderson, H.J. Burstein, H. Chew, C. Dang, J. Natl. Compr. Canc. Netw. **20**, 691–722 (2022)
16. O.C. Didamson, R. Chandran, H. Abrahamse, Cancers **14**, 4558 (2022). https://doi.org/10.3390/cancers14194558
17. F. Weiss, D. Lauffenburger, P. Friedl, Nat. Rev. Cancer. **22**, 157–173 (2022)
18. J.M. Breasted, *The Edwin Smith surgical papyrus* (University of Chicago Press, Chicago, 1930)
19. S.N. Goldberg, D.E. Dupuy, J Vasc Interv Radiol. **12**, 1021–1032 (2001)
20. M.H. Seegenschmiedt, L.W. Brady, R. Am, J Clin Oncol. **3**, 352–363 (1990)
21. F.W. Kremkau, J Clin Ultrasound. **7**, 287–300 (1979)
22. L.O. Svaasand, C.J. Gomer, E. Morinelli, Lasers Med Sci. **5**, 121–128 (1990)
23. P. Kaur, M.L. Aliru, A.S. Chadha, A. Asea, S. Krishnan, Int J Hyperthermia. **32**(1), 76–88 (2016). https://doi.org/10.3109/02656736.2015.1120889
24. A.N. Shipway, E. Katz, I. Willner, Chem. phys. chem. **1**, 18–52 (2000)
25. N.S. Abadeer, C.J. Murphy, J. Phys. Chem. C. **120**, 4691–4716 (2016)
26. E.Y. Lukianova-Hleb, E.Y. Hanna, J.H. Hafner, Nanotechnology **21**(8), 109501 (2010)
27. U. Kreibig, M. Vollmer, *Optical properties of metal clusters* (Springer, Berlin, 1995), pp.203–275
28. S. Vijayakumar, J. Saudi Chem. Soc. **23**, 753–761 (2019). https://doi.org/10.1016/j.jscs.2018.12.002
29. T. Mosmann, J. Immunol. Methods **65**, 55–63 (1983)
30. A. Gupta, S. Pandey, J.S. Yadav, Adv Pharm Bull. **11**, 10–27 (2021). https://doi.org/10.34172/apb.2021.002
31. A. Ghasemzadeh, N. Ghasemzadeh, J Med Plants Res. **5**(31), 6697–6703 (2011). https://doi.org/10.5897/JMPR11.1404
32. J. Conde, T.J. Dias, V. Grazu, M. Moros, V. Pedro, M.J. Fuente, Front Chem. **2**, 2 (2014). https://doi.org/10.3389/fchem.2014.00048
33. L. Ning, W. De-Ning, Y. Sheng-Kang, Macromolecules **30**, 4405–4409 (1997)
34. V. Lin, N. B. Colthup, W. G. Fateley, J. G. Grasselli. (Academic Press. Boston, 1991).
35. H.B. Sharif, B. Gabi, S.M. Abdullahi, Bayero J Pure Appl Sci. **10**(2), 57–63 (2018)

36. M.S. Davenport, M.A. Perazella, J. Yee, J.R. Dillman, D. Fine, R.J. McDonald, R.A. Rodby, C.L. Wang, J.C. Weinreb, Radiology **294**(3), 660–668 (2020). https://doi.org/10.1148/radiol.2019192094
37. D. Dastidar, D. Ghosh, G. Chakrabarti, Vessel Plus. **4**, 14 (2020). https://doi.org/10.20517/2574-1209.2019.36
38. W. Yang, H. Liang, S. Ma, D. Wang, J. Huang, Sustain Mater Technol. **22**, e00109 (2019). https://doi.org/10.1016/j.susmat.2019.e00109

Publisher's Note Springer Nature remains neutral with regard to jurisdictional claims in published maps and institutional affiliations.

Springer Nature or its licensor (e.g. a society or other partner) holds exclusive rights to this article under a publishing agreement with the author(s) or other rightsholder(s); author self-archiving of the accepted manuscript version of this article is solely governed by the terms of such publishing agreement and applicable law.